

Towards a Sampling Theory for Implicit Neural Representations

Mahrokh Najaf Gregory Ongie
Department of Mathematical and Statistical Sciences
Marquette University
Milwaukee, WI

Abstract—Implicit neural representations (INRs) have emerged as a powerful tool for solving inverse problems in computer vision and computational imaging. INRs represent images as continuous domain functions realized by a neural network taking spatial coordinates as inputs. However, unlike traditional pixel representations, little is known about the sample complexity of estimating images using INRs in the context of linear inverse problems. Towards this end, we study the sampling requirements for recovery of a continuous domain image from its low-pass Fourier coefficients by fitting a single hidden-layer INR with ReLU activation and a Fourier features layer using a generalized form of weight decay regularization. Our key insight is to relate minimizers of this non-convex parameter space optimization problem to minimizers of a convex penalty defined over an infinite-dimensional space of measures. We identify a sufficient number of samples for which an image realized by a width-1 INR is exactly recoverable by solving the INR training problem, and give a conjecture for the general width- W case. To validate our theory, we empirically assess the probability of achieving exact recovery of images realized by low-width single hidden-layer INRs, and illustrate the performance of INR on super-resolution recovery of more realistic continuous domain phantom images.

I. INTRODUCTION

Many inverse problems in signal and image processing are naturally posed in continuous domain. For example, in magnetic resonance imaging, measurements are modeled as samples of the Fourier transform of a function $f(\mathbf{x})$ defined over continuous spatial coordinates $\mathbf{x} \in \mathbb{R}^3$ [1]. Often these continuous domain inverse problems are approximated using discrete image or signal representations, along with an appropriate discretization of the forward model, such as the discrete Fourier transform in place of the continuous Fourier transform. However, this can lead to undesirable discretization artifacts, such as Gibb’s ringing [2], [3], [4], [5]. Such artifacts may be reduced by increasing the resolution of the discretization grid, but at the cost of additional computational complexity and potentially making the problem ill-posed without additional regularization.

Recently, continuous domain image representations using neural networks have gained traction in a variety of inverse problems arising in computer vision and computational imaging (see, e.g., the recent review [6]). These so-called *implicit neural representations* (INRs), also variously known as *coordinate-based neural networks* or *neural radiance fields*, parameterize a signal or image as a neural network defined over continuous spatial coordinates [7], [8], [9]. The main

benefits of INRs over discrete representations are that (1) they offer a compact (non-linear) representation of signals/images with far fewer parameters than a discrete representation, (2) they allow for more accurate continuous domain forward modeling, which can reduce the impact of discretization artifacts, and (3) standard neural network training can be used to fit an INR to measurements, sidestepping the need for custom iterative solvers.

However, the fundamental limits of image/signal estimation using INRs have not been explored in detail. One basic unanswered question is: How many linear measurements are necessary and sufficient for accurate reconstruction of a signal/image by fitting an INR? Additionally, how does the architecture of the INR influence the recovered signal/image? As a step in the direction of answering these questions, we consider the recovery of a signal/image from its low-pass Fourier coefficients using INRs. In particular, we focus on a popular INR architecture originally introduced in [9] that combines a fully-connected neural network with a Fourier features layer.

Recent work has shown that training a single hidden-layer ReLU network with ℓ^2 -regularization on its parameters (also known as “weight decay” regularization) imparts a sparsity effect, such that the network learned has low effective width [10], [11], [12], [13]. Bringing this perspective to INRs, we study the conditions under which a signal/image realizable by a single-hidden layer, low-width INR is exactly recoverable from low-pass Fourier samples by minimizing a generalized weight decay objective. Our main theoretical insight is to relate minimizers of this non-convex parameter space optimization problem to minimizers of a convex optimization problem posed over a space of measures. Using this framework, we identify a sufficient number of samples such that an image realizable by a width-1 INR is the unique minimizer of the INR training problem, and state a conjecture for widths greater than one. We validate this conjecture with numerical simulations. Finally, we illustrate the practical performance of INRs on super-resolution recovery of continuous domain phantom images, highlighting the impact of parameter-space regularization and network depth on recovery performance.

II. PROBLEM FORMULATION

We consider the recovery of a d -dimensional real-valued continuous domain signal/image $f : [0, 1]^d \rightarrow \mathbb{R}$ from a

sampling of its Fourier coefficients \hat{f} defined by

$$\hat{f}[\mathbf{k}] = \int_{[0,1]^d} f(\mathbf{x}) e^{-2\pi i \mathbf{k}^\top \mathbf{x}} d\mathbf{x},$$

where $\mathbf{k} \in \mathbb{Z}^d$ is any d -tuple of integer spatial frequencies. In particular, suppose we have access to all low-pass Fourier coefficients belonging to a uniformly sampled square region in frequency domain $\Omega = \{\mathbf{k} \in \mathbb{Z}^d : \|\mathbf{k}\|_\infty \leq K\}$ where K is a positive integer. Let $\mathcal{F}_\Omega f = (\hat{f}[\mathbf{k}])_{\mathbf{k} \in \Omega}$ denote the vector of Fourier coefficients of f restricted to Ω . We study the inverse problem of recovering the function f given $\mathbf{y} = \mathcal{F}_\Omega f$.

Clearly, this is an ill-posed inverse problem if no further assumptions are made on f . The INR approach attempts to resolve this ill-posedness by assuming f is well-approximated by a function realized by a ‘‘simple’’ neural network f_θ with trainable parameters θ . Under this assumption, one can attempt to recover f from measurements \mathbf{y} by solving the (non-linear) least squares problem

$$\min_{\theta} \frac{1}{2} \|\mathcal{F}_\Omega f_\theta - \mathbf{y}\|_2^2. \quad (1)$$

However, this problem may still be ill-posed (i.e., (1) may have multiple solutions) unless the number of trainable parameters used to define the INR f_θ is heavily constrained. Yet, useful solutions of (1) may be found by relying on implicit regularization induced by practical gradient-based algorithms [14].

As an alternative to using an overly constrained network architecture or relying on implicit regularization to resolve ill-posedness, we propose incorporating an explicit parameter space regularizer $C(\theta)$ to the least squares objective:

$$\min_{\theta} \frac{1}{2} \|\mathcal{F}_\Omega f_\theta - \mathbf{y}\|_2^2 + \lambda C(\theta), \quad (2)$$

where $\lambda > 0$ is a regularization parameter. In particular, we focus on a class of regularizers $C(\theta)$ that generalize *weight decay regularization*, the squared ℓ^2 -norm of all trainable parameters; this class is described in more detail below in Section II-B.

In a noise-free scenario, to tightly enforce data consistency constraints, the regularization parameter λ in (2) should be very small. As a model for this situation, we will focus on the equality constrained problem

$$\min_{\theta} C(\theta) \quad \text{s.t.} \quad \mathcal{F}_\Omega f_\theta = \mathbf{y}, \quad (3)$$

which can be thought of as the limiting case of (2) as $\lambda \rightarrow 0$. Our main goal is to characterize global minimizers of (3). In particular, we are interested in its *function space minimizers*, i.e., functions f_{θ^*} where θ^* is a global minimizer of (3). Given $\mathbf{y} = \mathcal{F}_\Omega f$ where f is realizable as an INR, we ask: when is f the unique function space minimizer of (3)? Next, we describe the architectural assumptions we put on the INR f_θ and the associated regularizer $C(\theta)$.

A. INR Architecture

We focus on an INR architecture first proposed in [9] that combines a trainable fully connected network with a Fourier features layer. For simplicity, we primarily consider a

‘‘shallow’’ INR architecture, where the fully connected network has a single-hidden layer with ReLU activation.

Specifically, consider a single-hidden layer ReLU network $g_\theta : \mathbb{R}^D \rightarrow \mathbb{R}$ of width- W as given by

$$g_\theta(\mathbf{y}) = \sum_{i=1}^W a_i [\mathbf{w}_i^\top \mathbf{y}]_+, \quad (4)$$

where $[t]_+ := \max\{0, t\}$ is the ReLU activation function, and $\theta = \{(a_i, \mathbf{w}_i)\}_{i=1}^W$ denotes the vector of all trainable parameters with $a_i \in \mathbb{R}$ and $\mathbf{w}_i \in \mathbb{R}^D$ for all $i \in [W]$. We denote the resulting parameter space by $\Theta_W \simeq \mathbb{R}^{W(D+1)}$. By choosing $D = d$, this architecture could be used as an INR directly. However, as shown in [9], it is challenging to recover high-frequency content in images using such an architecture.

To enhance recovery of high-frequency content, [9] proposed adding an initial Fourier features layer to the architecture. In this work, we focus on a Fourier features layer $\gamma : \mathbb{R}^d \rightarrow \mathbb{R}^D$ of the form

$$\gamma(\mathbf{x}) = [1, \sqrt{2} \cos(2\pi \mathbf{k}_1^\top \mathbf{x}), \dots, \sqrt{2} \cos(2\pi \mathbf{k}_p^\top \mathbf{x}), \sqrt{2} \sin(2\pi \mathbf{k}_1^\top \mathbf{x}), \dots, \sqrt{2} \sin(2\pi \mathbf{k}_p^\top \mathbf{x})]^\top, \quad (5)$$

where $\Omega_0 = \{\mathbf{k}_1, \dots, \mathbf{k}_p\} \subset \mathbb{R}^d$ is a collection of frequency vectors. For a single hidden-layer fully connected network, this gives the INR architecture:

$$f_\theta(\mathbf{x}) = g_\theta(\gamma(\mathbf{x})) = \sum_{i=1}^W a_i [\mathbf{w}_i^\top \gamma(\mathbf{x})]_+. \quad (6)$$

To better understand the impact of the Fourier features layer, for any weight vector $\mathbf{w} \in \mathbb{R}^D$, let us write $\mathbf{w} = [w^{(0)}, \mathbf{w}^{(1)}, \mathbf{w}^{(2)}]$ where $w^{(0)} \in \mathbb{R}$ and $\mathbf{w}^{(1)}, \mathbf{w}^{(2)} \in \mathbb{R}^p$. Then defining $\tau(\mathbf{x}) := \mathbf{w}^\top \gamma(\mathbf{x})$, we have

$$\tau(\mathbf{x}) = w^{(0)} + \sqrt{2} \sum_{j=1}^p \left(w_j^{(1)} \cos(2\pi \mathbf{k}_j^\top \mathbf{x}) + w_j^{(2)} \sin(2\pi \mathbf{k}_j^\top \mathbf{x}) \right).$$

This shows τ is a *trigonometric polynomial*, i.e., τ is a bandlimited function with frequency support contained in the discrete set Ω_0 . Therefore, a single-hidden layer INR with Fourier features layer is a weighted linear combination of functions of the form $\mathbf{x} \mapsto [\tau(\mathbf{x})]_+$. We call such a function a *rectified trigonometric polynomial*; see Figure 2 for an illustration.

Originally, [9] proposed defining the frequency set Ω_0 by sampling normally distributed random vectors $\mathbf{k} \sim \mathcal{N}(0, \sigma^2 \mathbf{I})$, where the variance σ is treated as a tunable parameter. To simplify the mathematical theory, in this work we focus on the case where Ω_0 consists of uniform sampled integer frequencies, i.e., $\Omega_0 = \{\mathbf{k} \in \mathbb{Z}^d : \|\mathbf{k}\|_\infty \leq K_0\}$. This implies that the INR is a periodic function on $[0, 1]^d$. Using uniformly sampled integer frequencies in place of random frequencies for an INR Fourier features layer was also investigated in [15].

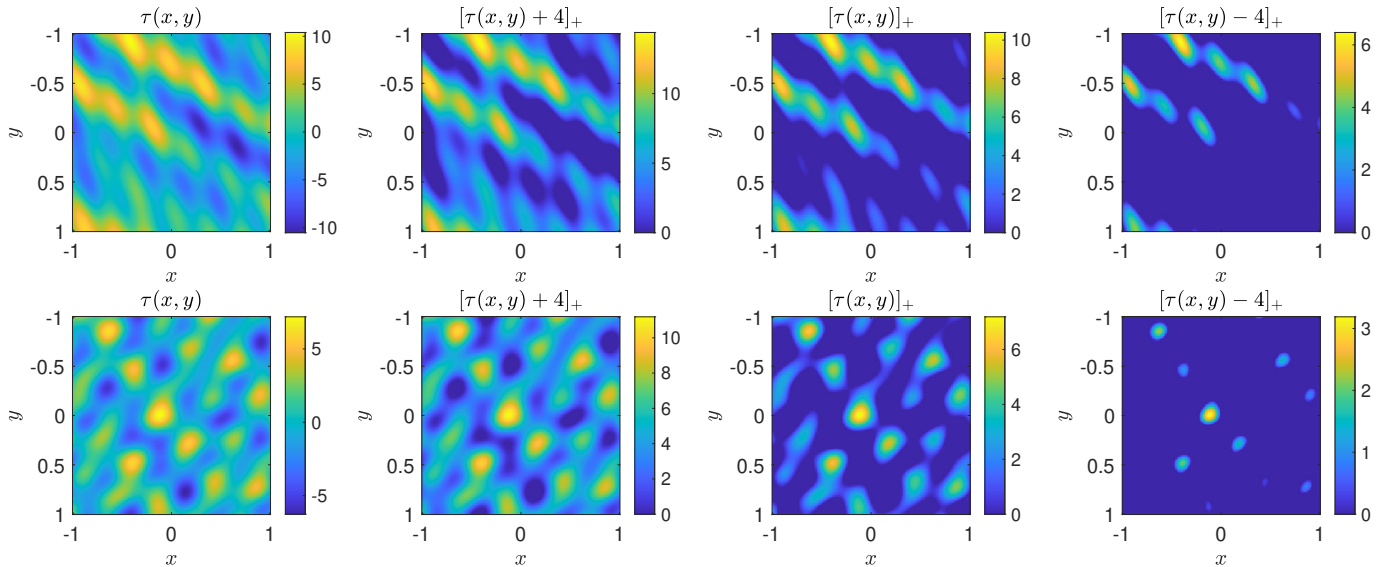


Fig. 1: The single-hidden layer INR architecture considered in this work represents an image f as a linear combination of rectified trigonometric polynomials $[\tau]_+$, as shown in the three columns on the right above. We study the sample complexity of estimating an image of this type from its low-pass Fourier coefficients.

B. Generalized Weight Decay Regularization

We focus on a family of parameter space regularizers $C(\theta)$ that strictly generalize “weight decay” regularization [16], i.e., the squared ℓ^2 -norm of all trainable parameters. Consider any non-negative *weighting function* η defined over inner-layer weight vectors $\mathbf{w} \in \mathbb{R}^D$. We say $\eta : \mathbb{R}^D \rightarrow [0, \infty)$ is an *admissible* weighting function if it satisfies the following properties:

- η is continuous.
- η is positive 1-homogeneous: $\eta(\alpha\mathbf{w}) = \alpha\eta(\mathbf{w})$ for all $\mathbf{w} \in \mathbb{R}^D$ and $\alpha \geq 0$.
- There exists a constant $B > 0$ such that $\eta(\mathbf{w}) \leq B\|\mathbf{w}\|_2$ for all $\mathbf{w} \in \mathbb{R}^D$.

Then, given any admissible weighting function η , we define the *generalized weight decay regularization* of any parameter vector $\theta = \{(a_i, \mathbf{w}_i)\}_{i=1}^W$ by

$$C(\theta) = \frac{1}{2} \sum_{i=1}^W (|a_i|^2 + \eta(\mathbf{w}_i)^2). \quad (7)$$

For example, if $\eta(\mathbf{w}) = \|\mathbf{w}\|_2$ we recover standard weight decay regularization. For the sampling theory given in Section III-C, we focus on the alternative weighting function

$$\eta(\mathbf{w}) = \|\mathcal{F}_\Omega[\mathbf{w}^\top \gamma(\cdot)]_+\|_2, \quad (8)$$

and call the resulting penalty $C(\theta)$ *modified weight decay regularization*. Note that we have $\|\mathcal{F}_\Omega[\mathbf{w}^\top \gamma(\cdot)]_+\|_2 \approx \|[\mathbf{w}^\top \gamma(\cdot)]_+\|_2$ assuming $\Omega \supseteq \Omega_0$, so modified weight decay regularization can be seen as approximately normalizing the L^2 -norm contribution made by each unit $[\mathbf{w}^\top \gamma(\cdot)]_+$ to the overall image.

III. THEORY

Our main theoretical insight is to show that minimizers of the non-convex INR training problem (3) coincide with minimizers of a *convex* optimization problem defined over an infinite-dimensional space of measures. We use this equivalence to prove our main theorem, which identifies a sufficient number of Fourier samples needed to recover a function realizable as a width-1 INR (i.e., a rectified trigonometric polynomial). Proofs of all results in this section are given in the Appendix.

A. Generalized Weight Decay Induces Unit Sparsity

Let $\Theta_W^* \subset \Theta_W$ denote the subset of parameter vectors $\theta = \{(a_i, \mathbf{w}_i)\}_{i=1}^W$ that satisfy the normalization constraint $\|\mathbf{w}_i\|_2 = 1$ for all $i \in [W]$. Then we have the following equivalence:

Lemma 1. *The function space minimizers of (3) coincide with the function space minimizers of*

$$\min_{\theta \in \Theta_W^*} \sum_{i=1}^W |a_i| \eta(\mathbf{w}_i) \text{ s.t. } \mathcal{F}_\Omega f_\theta = \mathbf{y}. \quad (9)$$

The proof follows by an argument similar to the proof of Lemma 1 in [10], and relies on the positive homogeneity of the ReLU activation and of the weighting function η . This result shows that by minimizing weight decay we implicitly minimize a weighted ℓ^1 -norm on the outer-layer weights a_i of the network subject to a normalization constraint on the inner-layer weight vectors \mathbf{w}_i . Due to the sparsity-promoting property of the ℓ^1 -norm, intuitively this result shows that by minimizing $C(\theta)$ we should promote functions that are realizable by a “sparse” INR, i.e., one with few active ReLU units.

B. Infinite-width Convexification

One technical hurdle to characterizing minimizers of (9) is that set of parameters $\theta \in \Theta_W^*$ satisfying the constraint $\mathcal{F}_\Omega f_\theta = \mathbf{y}$ is non-convex. To circumvent this issue, we show how to reformulate (9) as a convex optimization problem posed over a space of measures that represents the limit as the hidden-layer width $W \rightarrow \infty$. We note that similar convex formulations for single hidden-layer neural networks have been explored in [17], [18], [19].

First, observe that for any $\theta = (\{a_i, \mathbf{w}_i\}_{i=1}^W) \in \Theta_W^*$, by linearity we have

$$\mathcal{F}_\Omega f_\theta = \sum_{i=1}^W a_i \mathcal{F}_\Omega [\mathbf{w}_i^\top \gamma(\cdot)]_+. \quad (10)$$

We now show the sum on the right can be expressed as the integration of a function against a signed measure. In particular, define $\mathcal{U}_\eta = \{\mathbf{w} \in \mathbb{R}^D : \|\mathbf{w}\|_2 = 1, \eta(\mathbf{w}) > 0\}$. For any finite signed measure μ defined over \mathcal{U}_η , define the linear operator

$$\mathcal{K}_\Omega \mu := \int_{\mathcal{U}_\eta} \mathcal{F}_\Omega [\mathbf{w}_i^\top \gamma(\cdot)]_+ d\mu(\mathbf{w}). \quad (11)$$

Then for the sparse measure $\mu^* = \sum_{i=1}^W a_i \delta_{\mathbf{w}_i}$ where $\delta_{\mathbf{w}}$ denotes a Dirac delta measure centered at \mathbf{w} , we have $\mathcal{F}_\Omega f_\theta = \mathcal{K}_\Omega \mu^*$ and so the constraint $\mathcal{F}_\Omega f_\theta = \mathbf{y}$ in (9) is equivalent to $\mathcal{K}_\Omega \mu^* = \mathbf{y}$.

Next, define the weighted total variation norm $\|\mu\|_{TV, \eta}$ for any signed measure μ over \mathcal{U}_η by¹

$$\|\mu\|_{TV, \eta} = \int_{\mathcal{U}_\eta} \eta(\mathbf{w}) d|\mu|(\mathbf{w}),$$

where $|\mu|$ is the total variation measure associated with μ . Then we have $\|\mu^*\|_{TV, \eta} = \sum_{i=1}^W |a_i| \eta(\mathbf{w}_i)$ which coincides with the objective in (9).

Therefore, letting $\mathcal{M}_W(\mathcal{U}_\eta)$ denote the set of measures defined over \mathcal{U}_η expressible as a weighted linear combination of at most W Diracs, we have shown that (9) is equivalent to the optimization problem

$$P_W^* = \min_{\mu \in \mathcal{M}_W(\mathcal{U}_\eta)} \|\mu\|_{TV, \eta} \quad \text{s.t.} \quad \mathcal{K}_\Omega \mu = \mathbf{y}. \quad (12)$$

In particular, if the measure $\mu^* = \sum_{i=1}^W a_i \delta_{\mathbf{w}_i}$ is a minimizer of (12), then the parameter vector $\theta^* = \{(a_i, \mathbf{w}_i)\}_{i=1}^W \in \Theta_W^*$ is a minimizer of (9), and hence by Lemma 1, the INR f_{θ^*} is also a function space minimizer of the original INR training problem (3). This shows that we can describe all function space minimizers (3) by identifying the minimizers of (12).

However, analyzing (12) directly is challenging since domain $\mathcal{M}_W(\mathcal{U}_\eta)$ is not a vector space. To circumvent this issue, we pass to the larger space $\mathcal{M}(\mathcal{U}_\eta)$ of signed measures defined over \mathcal{U}_η with finite total variation norm, and consider the optimization problem

$$P^* = \min_{\mu \in \mathcal{M}(\mathcal{U}_\eta)} \|\mu\|_{TV, \eta} \quad \text{s.t.} \quad \mathcal{K}_\Omega \mu = \mathbf{y}. \quad (13)$$

¹By the admissibility conditions, η obeys the bound $\eta(\mathbf{w}) \leq B$ for all $\mathbf{w} \in \mathcal{U}_\eta$, which ensure the integral above is well-defined.

This can be thought of as the ‘‘infinite-width’’ analogue of (9). Note (13) is now a convex optimization problem, though one posed over an infinite dimensional space of measures.

Since $\mathcal{M}_W(\mathcal{U}_\eta) \subset \mathcal{M}(\mathcal{U}_\eta)$ we have $P^* \leq P_W^*$. Additionally, if a minimizer μ^* to (13) is a finite linear combination of at most W Diracs, i.e., $\mu^* \in \mathcal{M}_W(\mathcal{U}_\eta)$, then μ^* must also be a minimizer of (12), and so $P^* = P_W^*$. Our next result shows that, for sufficiently large training widths W , this is always the case.

Lemma 2. *Suppose $W \geq |\Omega|$. Then the minimums of (13) and (12) coincide, i.e., $P^* = P_W^*$, and $\mu^* \in \mathcal{M}_W(\mathcal{U}_\eta)$ is a minimizer of (13) if and only if μ^* is a minimizer of (12).*

This result implies that when $W \geq |\Omega|$, every sparse solution $\mu^* \in \mathcal{M}_W(\mathcal{U}_\eta)$ of (13) translates to function space minimizer of (3). In particular, if (13) has a unique solution, then it describes a unique function space minimizer of (3).

C. Provable Recovery of Width-1 INRs

Now we give our main theorem, which identifies a sufficient number of samples for which an image realizable as a width-1 INR is exactly recoverable as the unique global minimizer of (3). For technical reasons, here we focus on the modified weight decay regularizer $C(\theta)$ defined using the specific weighting function $\eta(\mathbf{w})$ given in (8). Also, we assume the Fourier feature frequency set $\Omega_0 = \{\mathbf{k} \in \mathbb{Z}^d : \|\mathbf{k}\|_\infty \leq K_0\}$, and for any positive integer n , we let $n\Omega$ denote the dilated frequency set $n\Omega_0 = \{\mathbf{k} \in \mathbb{Z}^d : \|\mathbf{k}\|_\infty \leq nK_0\}$. Then we have the following result:

Theorem 1. *Let $f(\mathbf{x}) = a[\tau]_+$ where τ is a real-valued trigonometric polynomial with frequency support in Ω_0 . Suppose $\Omega \supseteq 3\Omega_0$, and $\mathbf{y} = \mathcal{F}_\Omega f$. Then, assuming $W \geq |\Omega|$, f is the unique function space minimizer of the INR training problem (3) using modified weight decay regularization.*

The main idea of the proof is to pass to the convex dual of (13), which reduces to a semi-infinite program, i.e., a finite dimensional linear program with infinitely many constraints. Similar to previous works that have focused on super-resolution of sparse spikes [20], [21], [22], we prove unique recovery is equivalent to the construction of a particular dual optimal solution known as a *dual certificate*; see Appendix C for more details.

More generally, we conjecture that Theorem 1 can be extended to the case of standard weight decay regularization (i.e., weighting function $\eta(\mathbf{w}) = \|\mathbf{w}\|_2$). This is verified empirically in the next section. Additionally, when f is a width W INR, we conjecture that sampling over the frequency set $3W\Omega_0$ is sufficient to ensure f is the unique minimizer of (13), both with standard and modified weight decay regularization, provided its normalized inner-layer weight vectors \mathbf{w}_i ‘‘well-separated’’ in terms of their geodesic distance on the sphere.

IV. EXPERIMENTS

A. INR Training Details

Solving the equality constrained problem (3) directly is challenging. To approximate the continuous domain Fourier sampling operator \mathcal{F}_Ω , we implement a discretized version $\tilde{\mathcal{F}}_\Omega$ using DFTs applied to a rasterization of the INR onto a 1024×1024 pixel grid. Also, to approximate the equality constraint $\tilde{\mathcal{F}}_\Omega f_\theta = \mathbf{y}$, a simple approach is to minimize the regularized least squares formulation (2) with $\tilde{\mathcal{F}}_\Omega$ in place of \mathcal{F}_Ω for a small regularization parameter $\lambda > 0$, which is the approach we take in most of our experiments.

However, in the exact recovery experiments detailed below where higher accuracy solutions are desired, we also attempt to solve the equality constrained problem (3) using the Augmented Lagrangian (AL) method (see, e.g., [23, Ch 7]). Specifically, for INR parameters $\theta \in \Theta_W$, and $\mathbf{q} \in \mathbb{C}^{|\Omega|}$, $\sigma > 0$ define the AL function $L(\theta, \mathbf{q}, \sigma)$ by

$$L(\theta, \mathbf{q}, \sigma) := C(\theta) + \operatorname{Re}\langle \mathbf{q}, \tilde{\mathcal{F}}_\Omega f_\theta - \mathbf{y} \rangle + \frac{\sigma}{2} \|\tilde{\mathcal{F}}_\Omega f_\theta - \mathbf{y}\|_2^2.$$

Then starting from initializations \mathbf{q}_0 , and σ_0 , for $k = 0, 1, 2, \dots, K - 1$, we perform the updates

$$\theta_{k+1} = \arg \min_{\theta} \mathcal{L}(\theta, \mathbf{q}_k, \sigma_k) \quad (14)$$

$$\mathbf{q}_{k+1} = \mathbf{q}_k + \mu_k (\tilde{\mathcal{F}}_\Omega f_{\theta_k} - \mathbf{y}) \quad (15)$$

$$\sigma_{k+1} = \gamma \sigma_k \quad (16)$$

where $\gamma > 1$ is a fixed constant. To approximate the solution of the subproblem (14) we use a standard gradient-based INR training algorithm.

B. Exact Recovery Experiments

To validate the conjectured sampling guarantees, we generate random continuous domain images realizable as a single hidden-layer “teacher network” INR of varying widths W ; Figure 2 shows an example for $W = 3$. We investigate the maximum sampling frequency K needed to recover the image by solving the optimization problem (3) using a “student network” INR with the same architecture but larger width.

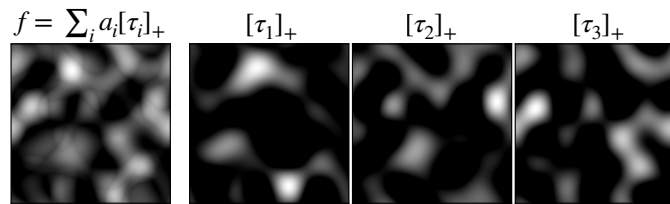


Fig. 2: Example of random width $W = 3$ “teacher” INR used in our exact recovery experiments. The image is a sum of the three randomly generated rectified trigonometric polynomials $[\tau_i]_+$ shown on the right.

For both the teacher and student networks, we use a Fourier features layer with maximum frequency $K_0 = 5$. We sweep over K values from 5 to 75 in increments of 5, while varying the teacher network width, W , from 1 to 5. For

each regularization approach and each (K, W) pair, we run 10 random trials. The width of student networks is 100. For standard weight decay regularization, we use AL parameters $\sigma_0 = 100$ and $\gamma = 2$, while for the modified weight decay regularization approach, we use $\sigma_0 = 10$ and $\gamma = 3$. For both regularization types, we perform $K = 20$ AL outer loop iterations, and run 5,000 iterations of the Adam optimizer with a learning rate of 0.001 to approximately minimize the AL inner loop subproblem (14). We say the recovery is “exact” if $\|\mathbf{f}_s - \mathbf{f}_t\|_\infty \leq 0.01$, where \mathbf{f}_s and \mathbf{f}_t are the discrete images output by the trained student INR and the teacher INR, respectively, evaluated on a 1024×1024 pixel grid.

Figure 3 shows the results of these experiments as probability tables. In the table corresponding to standard weight decay regularization, we see that the conjectured linear trend between the teacher network width W and the minimal sampling cutoff K needed to achieve exact recovery holds with high probability. However, modified weight decay regularization appears to fail for instances where $W > 2$. This suggests that standard weight decay regularization outperforms modified weight decay regularization at achieving exact recovery for $W > 2$. However, it is unclear whether this failure is due to fundamental limits to recovery, or in difficulties in solving the INR training problem to high precision with standard neural network optimization techniques. Despite this shortcoming, we note there still may be practical benefits to using modified weight decay regularization in achieving approximate recovery, as we show in the next set of experiments with more realistic phantom images.

C. Recovery of Continuous Domain Phantom Images

In Figure 4, we illustrate the use of INRs for the super-resolution recovery of two continuous domain phantoms whose Fourier coefficients are known exactly: a “dot phantom” image created for this study that features randomly generated circle-shaped features, and a piecewise constant MRI “brain phantom” introduced in [24]. The dot phantom is continuous, piecewise smooth, and exactly realizable by a shallow INR architecture of width $W \geq 50$ and $K_0 \geq 8$. Since the brain phantom is piecewise constant, and hence discontinuous, it is not exactly realizable with the INR considered in this work. We also note both phantoms are not bandlimited, such that a simple reconstruction obtained by zero-filling in Fourier domain and applying the IFFT results in significant ringing artifacts (see the second column in each panel of Figure 4).

For the dot phantom, the maximum sampling frequency is set to $K = 32$, and we fit a depth 2 INR with maximum frequency $K_0 = 10$ for the Fourier features layer and width 100. For the brain phantom, the maximum sampling frequency is set to $K = 64$, and we fit a depth 2 INR of width 500 with maximum frequency $K_0 = 20$ for the Fourier features layer. We train the INR by minimizing the regularized least squares formulation (2) using the Adam optimizer for 40,000 iterations with a learning rate of 0.001 followed by an additional 10,000 iterations with a learning rate of 0.0001.

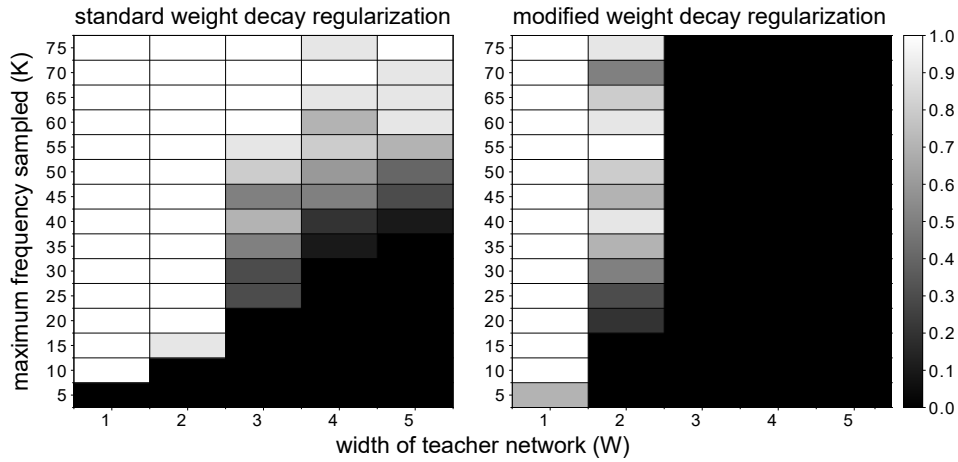


Fig. 3: Empirical probability of exact recovery of images representable by a single hidden-layer INR of width- W from its low-pass Fourier coefficients with maximum sampling frequency K by solving (3) using standard and modified weight decay regularization.

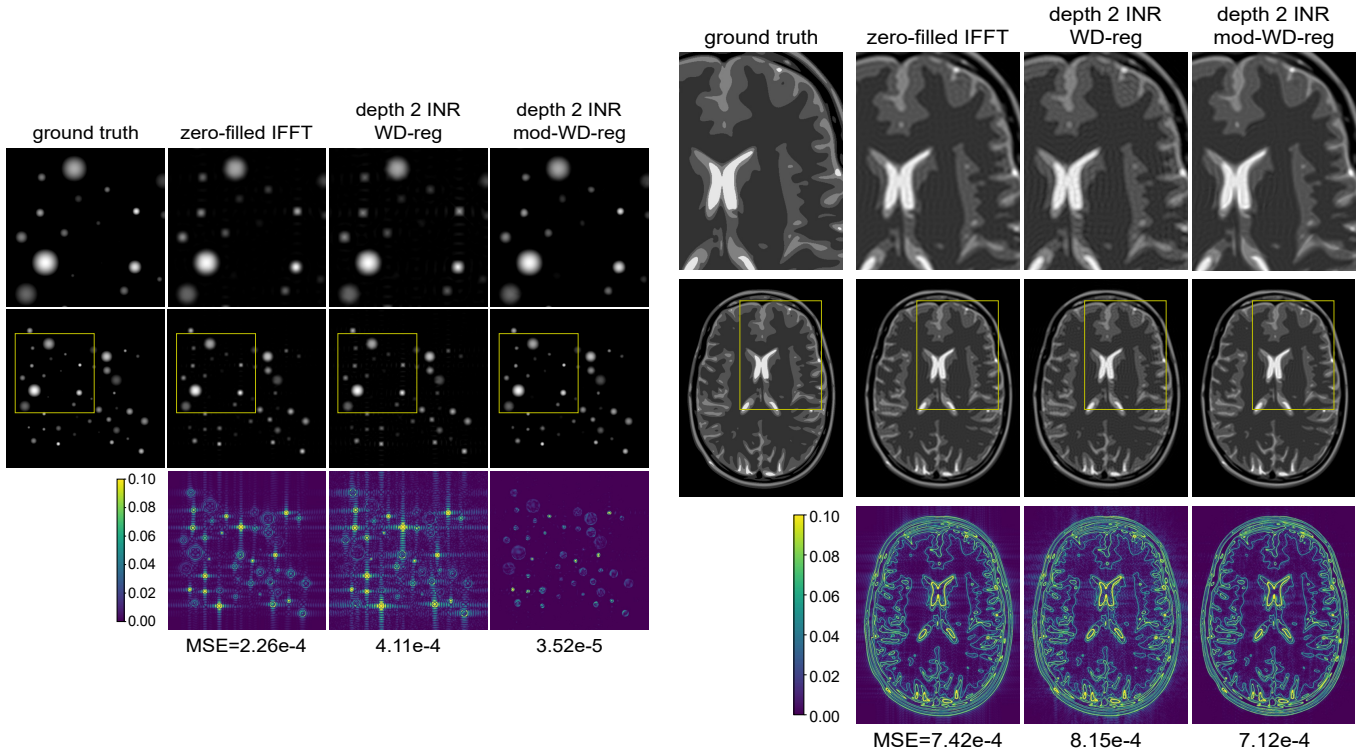


Fig. 4: **Recovery of continuous domain phantoms from low-pass Fourier samples.** Left panel: “dot phantom” image created for this study features randomly generated circle-shaped features. Right panel: piecewise constant brain MRI phantom introduced in [24]. We compare the zero-filled IFFT reconstruction with a single-hidden layer INR trained with standard weight decay regularization (depth 2 INR, WD-reg), and with the proposed modified weight decay regularization (depth 2 INR, mod-WD-reg). All grayscale images are shown on the scale $[0, 1]$. The bottom row shows the absolute value of the difference with the ground truth.

In each case, the regularization parameter λ was selected via grid search to minimize image domain MSE.

Unlike the exact recovery experiments, for both phantoms, we find that using a depth 2 INR trained with modified weight decay regularization results in lower image MSE and fewer artifacts in the reconstructions compared to standard weight decay regularization. In particular, the MSE is a magnitude lower on the dot phantom with modified weight decay and the reconstruction has far fewer ringing artifacts. A more modest improvement is shown on the brain phantom, where training with modified weight decay yields a slight improvement in MSE, but some ringing artifacts are still visible.

Additionally, in Figure 5, we demonstrate the impact of weight decay regularization strength on the reconstructed brain phantom images. First, we see that including weight decay regularization (i.e., setting $\lambda > 0$) yields reconstructions with lower image domain MSE and fewer visual ringing artifacts than training without regularization. However, using too large of a λ value yields an over-smoothed reconstruction. We also investigate the impact of regularization strength on the sparsity of the trained INR weights. In particular, given a ReLU unit of the form $a[\mathbf{w}^\top \gamma(\cdot)]_+$, we define its unit size to be $|a|\eta(\mathbf{w})$, where η is the weighting function used to define the generalized weight decay regularization term in (7). By Lemma 1, the sum of the unit sizes should be minimized when using generalized weight decay. From the histograms of the unit sizes shown in Figure 5, we see a large spread in unit sizes when not using regularization ($\lambda = 0$), while as we increase the regularization strength, the number of units with size close to zero increases markedly. The effect is especially pronounced for large λ in modified weight decay regularization, where nearly all unit sizes are clustered close to zero except for a few large outliers, indicating the trained INR has very low effective width.

D. Effect of Depth

Though our theory focuses on depth 2 INRs (i.e., single hidden-layer), we also explore the effect of depth on the induced image domain with and without weight decay regularization. Using the same setup as previously used for the brain phantom, in Figure 6 we show the results of fitting an INR with depths of 5, 10, and 15. These results show that with or without weight decay regularization, increasing INR depth results in lower image domain MSE and fewer ringing artifacts, indicating that deeper INRs may be biased towards piecewise constant (or piecewise smooth) reconstructions. Additionally, a comparison of the reconstructions in the first and second rows of Figure 6 demonstrates that training deep INR with weight decay regularization gives lower image domain MSE and visually improved reconstructions, showing that weight decay regularization can have benefits for recovery with deep INR networks, as well.

V. CONCLUSION

In this work, we introduce a mathematical framework for studying exact recovery of continuous domain images from

low-pass Fourier coefficients with INRs. We show that fitting a single-hidden layer INR architecture using a generalized weight decay regularization term is equivalent to a convex problem optimization defined over a space of measures. Using this perspective, we identify a sufficient number of samples to uniquely recover an image realizable as a width-1 INR, which we conjecture generalizes larger widths, as well.

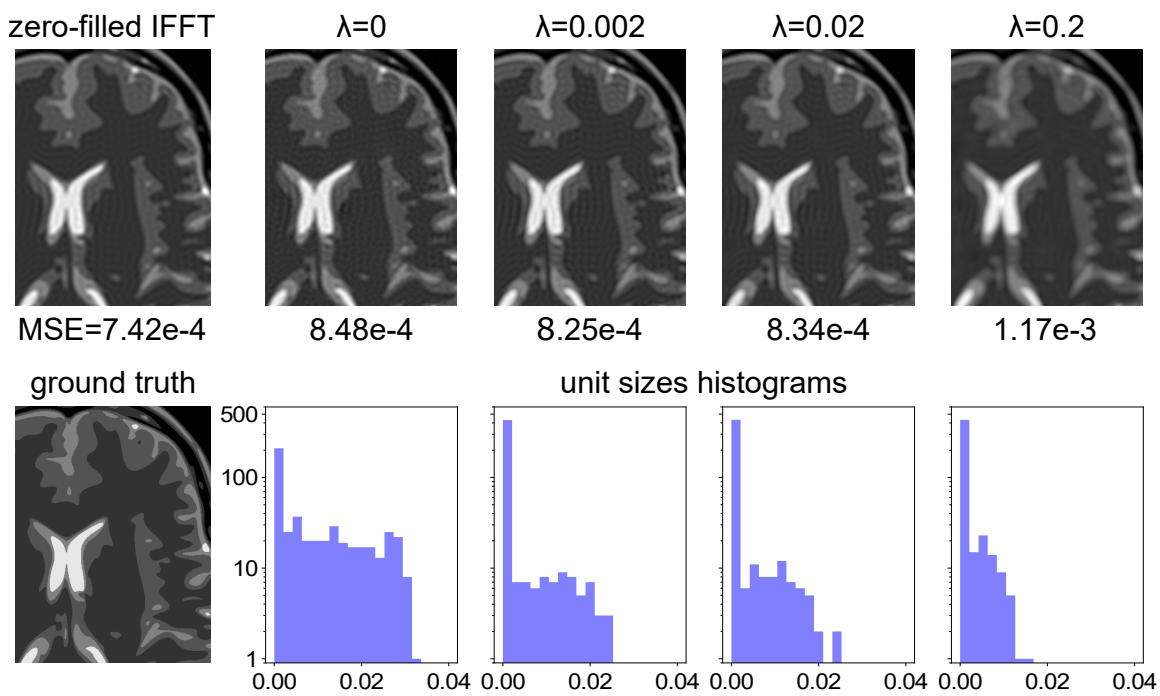
While this work focused on a specific INR architecture introduced in [9], several other architectures have been proposed as well [8], [25], [15], and extending the present results to these alternative architectures is an interesting direction for future work. Also, for mathematical tractability, we focused on a single hidden-layer INR architecture, but many studies use INR architectures with two or more hidden layers. Characterizing the function space regularization effect of deeper architectures will also be a focus of future work.

ACKNOWLEDGMENT

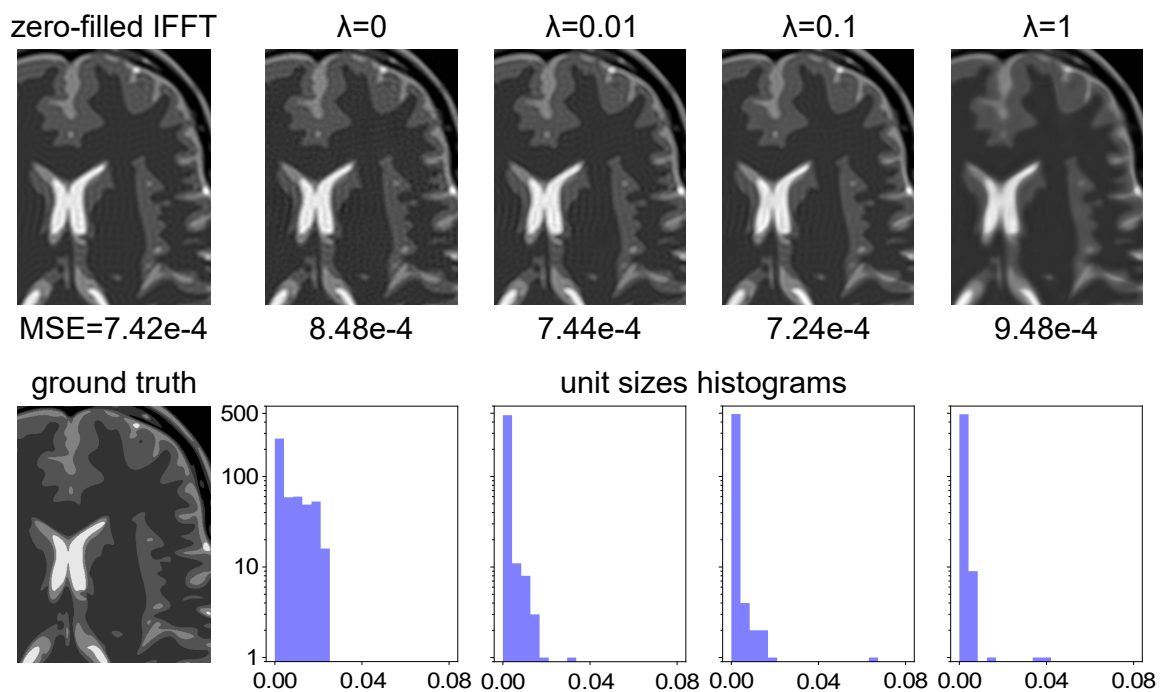
This work was supported by NSF CRII award CCF-2153371.

REFERENCES

- [1] J. A. Fessler, "Model-based image reconstruction for MRI," *IEEE signal processing magazine*, vol. 27, no. 4, pp. 81–89, 2010.
- [2] R. Archibald and A. Gelb, "A method to reduce the Gibbs ringing artifact in MRI scans while keeping tissue boundary integrity," *IEEE Transactions on Medical Imaging*, vol. 21, no. 4, pp. 305–319, 2002.
- [3] J. Veraart, E. Fieremans, I. O. Jelescu, F. Knoll, and D. S. Novikov, "Gibbs ringing in diffusion MRI," *Magnetic resonance in medicine*, vol. 76, no. 1, pp. 301–314, 2016.
- [4] G. Ongie and M. Jacob, "Recovery of piecewise smooth images from few fourier samples," pp. 543–547, 2015.
- [5] —, "Off-the-grid recovery of piecewise constant images from few fourier samples," *SIAM Journal on Imaging Sciences*, vol. 9, no. 3, pp. 1004–1041, 2016.
- [6] Y. Xie, T. Takikawa, S. Saito, O. Litany, S. Yan, N. Khan, F. Tombari, J. Tompkin, V. Sitzmann, and S. Sridhar, "Neural fields in visual computing and beyond," in *Computer Graphics Forum*, vol. 41, no. 2. Wiley Online Library, 2022, pp. 641–676.
- [7] B. Mildenhall, P. P. Srinivasan, M. Tancik, J. T. Barron, R. Ramamoorthi, and R. Ng, "Nerf: Representing scenes as neural radiance fields for view synthesis," *Communications of the ACM*, vol. 65, no. 1, pp. 99–106, 2021.
- [8] V. Sitzmann, J. Martel, A. Bergman, D. Lindell, and G. Wetzstein, "Implicit neural representations with periodic activation functions," *Advances in Neural Information Processing Systems*, vol. 33, pp. 7462–7473, 2020.
- [9] M. Tancik, P. Srinivasan, B. Mildenhall, S. Fridovich-Keil, N. Raghavan, U. Singhal, R. Ramamoorthi, J. Barron, and R. Ng, "Fourier features let networks learn high frequency functions in low dimensional domains," *Advances in Neural Information Processing Systems*, vol. 33, pp. 7537–7547, 2020.
- [10] P. Savarese, I. Evron, D. Soudry, and N. Srebro, "How do infinite width bounded norm networks look in function space?" in *Conference on Learning Theory*. PMLR, 2019, pp. 2667–2690.
- [11] G. Ongie, R. Willett, D. Soudry, and N. Srebro, "A function space view of bounded norm infinite width relu nets: The multivariate case," in *International Conference on Learning Representations*, 2019.
- [12] R. Parhi and R. D. Nowak, "Banach space representer theorems for neural networks and ridge splines," *Journal of Machine Learning Research*, vol. 22, no. 43, pp. 1–40, 2021.
- [13] —, "Deep learning meets sparse regularization: A signal processing perspective," *IEEE Signal Processing Magazine*, vol. 40, no. 6, pp. 63–74, 2023.
- [14] S. Gunasekar, J. Lee, D. Soudry, and N. Srebro, "Characterizing implicit bias in terms of optimization geometry," in *International Conference on Machine Learning*. PMLR, 2018, pp. 1832–1841.



(a) standard weight decay regularization



(b) modified weight decay regularization

Fig. 5: **Impact of regularization on brain phantom reconstructions and unit sizes of a trained depth 2 INR.** In the first row of each panel, we compare the zero-filled IFFT reconstruction with the reconstructions obtained with a depth 2 INR trained with standard/modified weight decay regularization for different values of regularization strength λ . The histograms in the second row of each panel represent the distribution of unit sizes $\{|a_i|\eta(\mathbf{w}_i)\}_{i=1}^{500}$ of the trained INRs across different values of λ . As λ increases, the unit sizes cluster at zero, indicating the trained INR is sparse in the sense that it has a few active units.

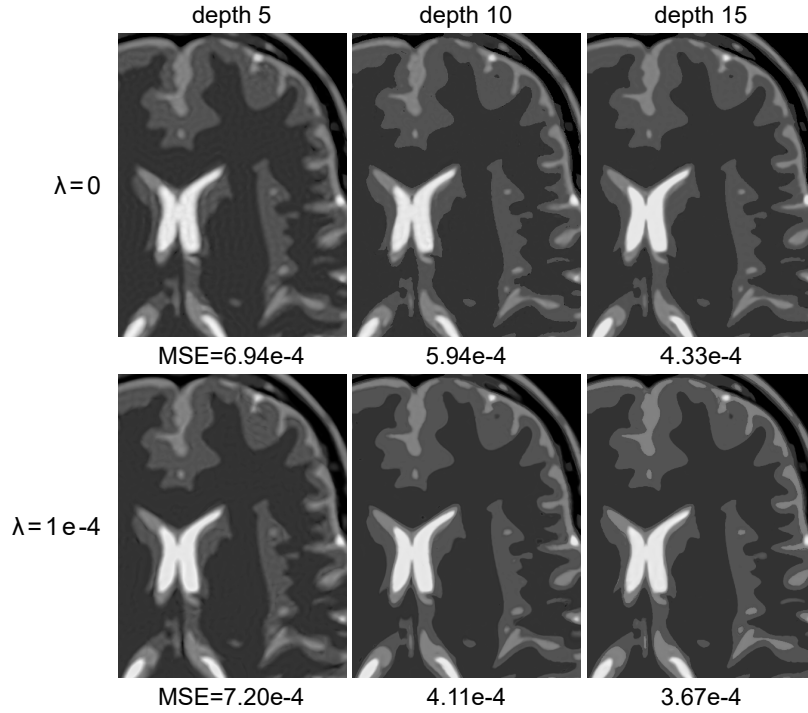


Fig. 6: **Effect of INR depth on image recovery.** Top row: reconstructions using no regularization ($\lambda = 0$). Bottom row: reconstructions using standard weight decay regularization ($\lambda = 1e-4$). Increasing the INR depth leads to lower image domain MSE and less visible ringing artifacts and sharp edges. Additionally, for each depth, a visible improvement in the quality of reconstructions is observed when using weight decay regularization.

- [15] N. Benbarka, T. Höfer, A. Zell *et al.*, “Seeing implicit neural representations as fourier series,” in *Proceedings of the IEEE/CVF Winter Conference on Applications of Computer Vision*, 2022, pp. 2041–2050.
- [16] A. Krogh and J. Hertz, “A simple weight decay can improve generalization,” *Advances in neural information processing systems*, vol. 4, 1991.
- [17] Y. Bengio, N. Roux, P. Vincent, O. Delalleau, and P. Marcotte, “Convex neural networks,” *Advances in neural information processing systems*, vol. 18, 2005.
- [18] F. Bach, “Breaking the curse of dimensionality with convex neural networks,” *Journal of Machine Learning Research*, vol. 18, no. 19, pp. 1–53, 2017.
- [19] T. Ergen and M. Pilanci, “Convex geometry and duality of over-parameterized neural networks,” *Journal of machine learning research*, vol. 22, no. 212, pp. 1–63, 2021.
- [20] E. J. Candès and C. Fernandez-Granda, “Towards a mathematical theory of super-resolution,” *Communications on pure and applied Mathematics*, vol. 67, no. 6, pp. 906–956, 2014.
- [21] C. Poon and G. Peyré, “Multidimensional sparse super-resolution,” *SIAM Journal on Mathematical Analysis*, vol. 51, no. 1, pp. 1–44, 2019.
- [22] A. Eftekhari, T. Bendory, and G. Tang, “Stable super-resolution of images: theoretical study,” *Information and Inference: A Journal of the IMA*, vol. 10, no. 1, pp. 161–193, 2021.
- [23] J. Nocedal and S. J. Wright, *Numerical optimization*. Springer.
- [24] M. Guerquin-Kern, L. Lejeune, K. P. Pruessmann, and M. Unser, “Realistic analytical phantoms for parallel magnetic resonance imaging,” *IEEE Transactions on Medical Imaging*, vol. 31, no. 3, pp. 626–636, 2011.
- [25] T. Müller, A. Evans, C. Schied, and A. Keller, “Instant neural graphics primitives with a multiresolution hash encoding,” *ACM transactions on graphics (TOG)*, vol. 41, no. 4, pp. 1–15, 2022.
- [26] K. Bredies and M. Carioni, “Sparsity of solutions for variational inverse problems with finite-dimensional data,” *Calculus of Variations and Partial Differential Equations*, vol. 59, no. 1, p. 14, 2020.
- [27] C. Zalinescu, *Convex analysis in general vector spaces*. World scientific, 2002.
- [28] Y. De Castro and F. Gamboa, “Exact reconstruction using beurling minimal extrapolation,” *Journal of Mathematical Analysis and applications*, vol. 395, no. 1, pp. 336–354, 2012.

APPENDIX

A. Proof of Lemma 1

Given any parameter vector $\theta = ((a_i, \mathbf{w}_i))_{i=1}^W \in \Theta_W$ we construct a new parameter vector $\theta' = ((a'_i, \mathbf{w}'_i))_{i=1}^W \in \Theta_W$ to satisfy $f_\theta = f_{\theta'}$ as follows: For all i such that $\eta(\mathbf{w}_i) > 0$, define $c_i = \sqrt{|a_i|/\eta(\mathbf{w}_i)}$, and set $a'_i = a_i/c_i$ and $\mathbf{w}'_i = c_i \mathbf{w}_i$. For all i such that $\eta(\mathbf{w}_i) = 0$, set $\mathbf{w}'_i = \mathbf{0}$ and $a'_i = 0$. Then, by positive 1-homogeneity of both the ReLU activation and of η , and by the fact that $\eta(\mathbf{w}_i) = 0$ if and only if $[\mathbf{w}_i^\top \gamma(\cdot)]_+$ is identically zero, we see that $a'_i [\mathbf{w}'_i{}^\top \gamma(\cdot)]_+ = a_i [\mathbf{w}_i^\top \gamma(\cdot)]_+$ for all i , and so $f_\theta = f_{\theta'}$.

Now, by the inequality of arithmetic means and geometric means, we have

$$C(\theta) = \frac{1}{2} \sum_{i=1}^W (|a_i|^2 + \eta(\mathbf{w}_i)^2) \geq \sum_{i=1}^W |a_i| \eta(\mathbf{w}_i) = C(\theta').$$

This shows that every parameter vector $\theta \in \Theta_W$ feasible for (3) can be mapped to another parameter vector $\theta' \in \Theta_W$ feasible for (3) that achieves the modified cost $\sum_{i=1}^W |a_i| \eta(\mathbf{w}_i)$ which is also a lower bound on $C(\theta)$. Therefore, we see that (3) has the same minimizers as

$$\min_{\theta \in \Theta_W} \sum_{i=1}^W |a_i| \eta(\mathbf{w}_i) \quad \text{s.t.} \quad \mathcal{F}_\Omega f_\theta = \mathbf{y}.$$

Finally, since the quantity $|a_i|\eta(\mathbf{w}_i)$ is invariant to the re-scaling $\mathbf{w}_i \mapsto \mathbf{w}_i/\|\mathbf{w}_i\|$ and $a_i \mapsto \| \mathbf{w}_i \| a_i$, and this re-scaling of parameters realizes the same INR, we may additionally constrain the optimization to all parameter vectors satisfying $\|\mathbf{w}_i\| = 1$ for all $i \in [W]$, i.e., to all $\theta \in \Theta_W^*$, which gives the equivalence with the optimization problem in Lemma 1.

B. Proof of Lemma 2

To prove Lemma 2, we apply the abstract representer theorem of [26, Theorem 3.3]. A simplified version of this result is stated as follows: if ϕ is a norm on a locally convex space \mathcal{X} , and $\mathcal{A} : \mathcal{X} \rightarrow H$ is a continuous linear operator mapping surjectively onto a finite dimensional Hilbert space H , then given any $y \in H$ the optimization problem

$$\min_{x \in \mathcal{X}} \phi(x) \quad \text{s.t.} \quad \mathcal{A}x = y$$

has a minimizer of the form $x^* = \sum_{i=1}^p a_i u_i$ where $p \leq \dim H$, $a_i \in \mathbb{R}$, and u_i are extremal points of the unit ball $\{x \in \mathcal{X} : \phi(x) \leq 1\}$.

In the present setting, we consider the locally convex space $\mathcal{X} = \mathcal{M}(\mathcal{U}_\eta)$ of finite signed measures over \mathcal{U}_η equipped with the weak-* topology, the norm $\phi = \|\cdot\|_{TV,\eta}$, and the linear operator $\mathcal{A} = \mathcal{K}_\Omega$ mapping into $H = \mathbb{C}_{sym}(\Omega)$, the space of complex-valued conjugate symmetric arrays indexed by Ω , which is isomorphic to $\mathbb{R}^{|\Omega|}$.

By a similar argument to [26, Theorem 4.2], the set of extreme points of the unit ball $\{\mu \in \mathcal{M}(\mathcal{U}_\eta) : \|\mu\|_{TV,\eta} \leq 1\}$ coincides with the set of scaled Dirac measures $\{\pm \eta(\mathbf{w})^{-1} \delta_{\mathbf{w}} : \mathbf{w} \in \mathcal{U}_\eta\}$. Hence, assuming \mathcal{K}_Ω is continuous and surjective, we see that (13) has a sparse solution $\mu^* = \sum_{i=1}^p a_i \delta_{\mathbf{w}_i}$ where $a_i \in \mathbb{R}$ and $\mathbf{w}_i \in \mathcal{U}_\eta$, and $p \leq \dim_{\mathbb{R}} \mathbb{C}_{sym}(\Omega) = |\Omega|$. Therefore, if $W \geq |\Omega|$, this implies $\theta^* = \{(a_i, \mathbf{w}_i)\}_{i=1}^W$ is a minimizer of (12) and so $P_W^* = P^*$, as claimed.

Therefore, all that remains so show is that $K_\Omega : \mathcal{M}(\mathcal{U}_\eta) \rightarrow \mathbb{C}_{sym}(\Omega)$ is continuous and surjective. First, to prove continuity, it suffices to show K_Ω is the adjoint of a bounded linear operator $\mathcal{L}_\Omega : \mathbb{C}_{sym}(\Omega) \rightarrow \mathcal{C}_0(\mathcal{U}_\eta)$, where the $\mathcal{C}_0(\mathcal{U}_\eta)$ is the space of continuous functions on \mathcal{U}_η vanishing on the boundary $\partial\mathcal{U}_\eta$ equipped with the supremum norm, which is pre-dual to $\mathcal{M}(\mathcal{U}_\eta)$. In particular, consider the linear operator $\mathcal{L}_\Omega : \mathbb{C}_{sym}(\Omega) \rightarrow \mathcal{C}(\mathcal{U}_\eta)$ defined for any $\mathbf{z} \in \mathbb{C}_{sym}(\Omega)$ by

$$[\mathcal{L}_\Omega \mathbf{z}](\mathbf{w}) = \langle F_\Omega[\mathbf{w}^\top \boldsymbol{\gamma}(\cdot)]_+, \mathbf{z} \rangle \quad \forall \mathbf{w} \in \mathcal{U}_\eta.$$

By the Cauchy-Schwartz inequality, we have

$$|[\mathcal{L}_\Omega \mathbf{z}](\mathbf{w})| \leq \|F_\Omega[\mathbf{w}^\top \boldsymbol{\gamma}(\cdot)]_+\|_2 \|\mathbf{z}\|_2,$$

and by Parseval's Theorem, we have the bound

$$\begin{aligned} \|F_\Omega[\mathbf{w}^\top \boldsymbol{\gamma}(\cdot)]_+\|_2 &\leq \|[\mathbf{w}^\top \boldsymbol{\gamma}(\cdot)]_+\|_{L^2([0,1]^d)} \\ &\leq \|\mathbf{w}^\top \boldsymbol{\gamma}(\cdot)\|_{L^2([0,1]^d)} \\ &\leq \|\mathbf{w}\|_2 = 1. \end{aligned}$$

Therefore, $|[\mathcal{L}_\Omega \mathbf{z}](\mathbf{w})| \leq \|\mathbf{z}\|_2$ for all $\mathbf{w} \in \mathcal{U}_\eta$, which shows \mathcal{L}_Ω is a bounded linear operator. Next, for any $\mathbf{z} \in \mathbb{C}_{sym}(\Omega)$ and $\mu \in \mathcal{M}(\mathcal{U}_\eta)$, we have

$$\langle \mu, \mathcal{L}_\Omega \mathbf{z} \rangle = \int_{\mathcal{U}_\eta} [\mathcal{L}_\Omega \mathbf{z}](\mathbf{w}) d\mu \quad (17)$$

$$= \int_{\mathcal{U}_\eta} \langle F_\Omega[\mathbf{w}^\top \boldsymbol{\gamma}(\cdot)]_+, \mathbf{z} \rangle d\mu(\mathbf{w}) \quad (18)$$

$$= \left\langle \int_{\mathcal{U}_\eta} F_\Omega[\mathbf{w}^\top \boldsymbol{\gamma}(\cdot)]_+, d\mu(\mathbf{w}), \mathbf{z} \right\rangle \quad (19)$$

$$= \langle \mathcal{K}_\Omega \mu, \mathbf{z} \rangle \quad (20)$$

which proves $\mathcal{K}_\Omega = \mathcal{L}_\Omega^*$, as claimed.

Finally, we show that \mathcal{K}_Ω is surjective. For this, it suffices to show \mathcal{L}_Ω has a trivial nullspace, since this will imply $|\Omega| = \text{rank } \mathcal{L}_\Omega = \text{rank } \mathcal{L}_\Omega^* = \text{rank } \mathcal{K}_\Omega$. Towards this end, suppose $\mathbf{z} \in \mathbb{C}_{sym}(\Omega)$ non-zero. Then we will show $[\mathcal{L}_\Omega \mathbf{z}](\mathbf{w})$ is always non-zero for some value of $\mathbf{w} \in \mathcal{U}_\eta$. First, observe that

$$[\mathcal{L}_\Omega \mathbf{z}](\mathbf{w}) = \langle F_\Omega[\mathbf{w}^\top \boldsymbol{\gamma}(\cdot)]_+, \mathbf{z} \rangle \quad (21)$$

$$= \int_{[0,1]^d} [\mathbf{w}^\top \boldsymbol{\gamma}(\mathbf{x})]_+ [F_\Omega^* \mathbf{z}](\mathbf{x}) d\mathbf{x} \quad (22)$$

Define $\rho = F_\Omega^* \mathbf{z}$, which is a real-valued trigonometric polynomial. Without loss of generality, assume its positive set $P = \{\mathbf{x} \in (0,1)^d : \rho(\mathbf{x}) > 0\}$ is non-empty. By continuity of ρ , P is also an open set, and so it contains an open ball $B(\mathbf{x}_0, \epsilon)$ for some radius $\epsilon > 0$. Consider the translated sinc function $s(\mathbf{x}) := \text{sinc}_\Omega(\mathbf{x} - \mathbf{x}_0) - \alpha$, where we define $\text{sinc}_\Omega := F_\Omega^* \mathbf{1}$, and $\alpha > 0$ is a constant. Under our assumptions on the frequency set Ω , $\text{sinc}_\Omega(\mathbf{x})$ is a product of 1-D sinc functions, hence has a strict global maximum occurring at $\mathbf{x} = \mathbf{0}$. In particular, we may take α sufficiently close to $\text{sinc}_\Omega(\mathbf{0})$ such that $[s]_+$ is non-zero with support contained in $B(\mathbf{x}_0, \epsilon)$. Also, since $s(\mathbf{x})$ is a trigonometric polynomial bandlimited Ω_0 , there exists a vector $\mathbf{w}_0 \in \mathbb{R}^D$ such that $s(\mathbf{x}) = \mathbf{w}_0^\top \boldsymbol{\gamma}(\mathbf{x})$. Defining $\mathbf{w} = \mathbf{w}_0/\|\mathbf{w}_0\|_2$, we see that

$$[\mathcal{L}_\Omega \mathbf{z}](\mathbf{w}) = \|\mathbf{w}_0\|_2^{-1} \int_{[0,1]^d} [s(\mathbf{x})]_+ \rho(\mathbf{x}) d\mathbf{x} > 0,$$

as claimed.

C. Description of the Dual Problem

The function space optimization problem (13) is convex. We now describe the associated convex dual problem². A direct application of the Fenchel-Rockafellar duality theorem [27, Corollary 2.8.5] gives the following:

Lemma 3. *The dual problem associated with (13) is*

$$D^* = \sup_{\mathbf{z} \in \mathbb{C}_{sym}(\Omega)} \text{Re}\langle \mathbf{y}, \mathbf{z} \rangle \quad \text{s.t.} \quad |[\mathcal{L}_\Omega \mathbf{z}](\mathbf{w})| \leq \eta(\mathbf{w}) \quad \forall \mathbf{w} \in \mathcal{U}_\eta, \quad (23)$$

and strong duality holds, i.e., $D^* = P^*$ where P^* is the minimum of (13).

²Technically speaking, this is the pre-dual problem, since the space $\mathcal{M}(\mathcal{U}_\eta)$ is not reflexive. However, formally it has a similar structure to a convex dual.

For space reasons, we omit a full proof, but the key step is to use the following dual characterization of the weighted total variation norm:

$$\|\mu\|_{TV,\eta} = \sup_{\substack{\phi \in \mathcal{C}_0(\mathcal{U}_\eta) \\ |\phi(\mathbf{w})| \leq \eta(\mathbf{w}), \forall \mathbf{w} \in \mathcal{U}_\eta}} \int \phi(\mathbf{w}) d\mu(\mathbf{w}),$$

which allows us to identify $\|\mu\|_{TV,\eta}$ as the convex conjugate of the indicator function $\chi_C(\phi)$ where $C = \{\phi \in \mathcal{C}_0(\mathcal{U}_\eta) : |\phi(\mathbf{w})| \leq \eta(\mathbf{w}), \forall \mathbf{w} \in \mathcal{U}_\eta\}$.

Now we show how the existence of a particular dual feasible variable \mathbf{z} ensures optimality of a sparse measure for the primal problem (13). Suppose $\mathbf{y} = \mathcal{F}_\Omega f$ where $f(\mathbf{x}) = \sum_{i=1}^W a_i [\mathbf{w}_i^\top \gamma(\mathbf{x})]_+$ such that $a_i \neq 0$, $\mathbf{w}_i \in \mathcal{U}_\eta$ for all $i \in [W]$, and which is a minimal representation in the sense that for $\mu = \sum_{i=1}^W a_i \delta_{\mathbf{w}_i}$ we have $\|\mu\|_{TV,\eta} = \sum_{i=1}^W |a_i| \eta(\mathbf{w}_i)$. Define $\phi = \mathcal{L}_\Omega \mathbf{z}$. Then by linearity, we have

$$\begin{aligned} \langle \mathbf{y}, \mathbf{z} \rangle &= \langle \mathcal{F}_\Omega f, \mathbf{z} \rangle \\ &= \sum_{i=1}^W a_i \langle \mathcal{F}_\Omega [\mathbf{w}_i^\top \gamma(\cdot)]_+, \mathbf{z} \rangle \\ &= \sum_{i=1}^W a_i \phi(\mathbf{w}_i). \end{aligned}$$

Therefore, if there exists a dual feasible \mathbf{z} such that $\phi = \mathcal{L}^* \mathbf{z}$ satisfies $\phi(\mathbf{w}_i) = \text{sign}(a_i) \eta(\mathbf{w}_i)$ for all $i \in [W]$, we see that

$$\langle \mathbf{y}, \mathbf{z} \rangle = \sum_{i=1}^W |a_i| \eta(\mathbf{w}_i) = \|\mu\|_{TV,\eta}$$

i.e., the dual objective matches the primal objective, and so μ is a global minimizer of (13).

However, this argument does not determine whether μ is the unique global minimizer. A stronger condition that guarantees uniqueness is as follows:

Lemma 4. *Suppose $\mu = \sum_{i=1}^W a_i \delta_{\mathbf{w}_i}$ is primal feasible. Suppose there exists dual feasible variable \mathbf{z} such that $\phi = \mathcal{L}_\Omega \mathbf{z}$ satisfies*

$$\phi(\mathbf{w}_i) = \text{sign}(a_i) \eta(\mathbf{w}_i) \text{ for all } i = 1, \dots, W,$$

and $|\phi(\mathbf{w})| < 1$ otherwise. Then μ is the unique minimizer of (13).

We omit the full details of the proof, which is a variation on standard arguments for sparse measure recovery (see, e.g., [28], [20]). Following the convention in this literature, we call function ϕ appearing in Lemma 4 a *dual certificate* for μ .

D. Proof of Theorem 1

Before giving the proof of Theorem 1, we state the following key lemma, which shows that a rectified trigonometric polynomial is uniquely identifiable from sufficiently many of its low-pass Fourier coefficients:

Lemma 5. *Suppose $\Omega \supseteq 3\Omega_0$. Then the map $\mathbf{w} \mapsto \mathcal{F}_\Omega([\mathbf{w}^\top \gamma(\cdot)]_+)$ is injective over \mathcal{U}_η .*

We omit a full proof for space reasons. The basis of the proof is to make use of the fact that for any $\tau(\mathbf{x}) = \mathbf{w}^\top \gamma(\mathbf{x})$, and any $\varphi(\mathbf{x}) = \mathbf{v}^\top \gamma(\mathbf{x})$ with $\mathbf{w}, \mathbf{v} \in \mathcal{U}_\eta$, the equation

$$F_\Omega(\varphi \cdot \nabla[\tau]_+ - \nabla\varphi \cdot [\tau]_+) = 0$$

holds for $\mathbf{w} = \mathbf{v}$. The left-hand side is expressible as a linear operator acting on $\mathbf{v} = \hat{\varphi}$, which we show has nullspace of dimension one spanned by \mathbf{w} when $\Omega \supseteq 3\Omega_0$.

Now we give the proof of our main result.

Proof of Theorem 1. Let $\eta(\mathbf{w}) = \|\mathcal{F}_\Omega[\mathbf{w}^\top \gamma(\cdot)]_+\|_2$ and $f = a[\tau]_+$. Without loss of generality, we may assume $\tau(\mathbf{x}) = \mathbf{w}_0^\top \gamma(\mathbf{x})$ for some vector $\mathbf{w}_0 \in \mathcal{U}_\eta$, so that $f = a[\mathbf{w}_0^\top \gamma(\cdot)]_+$. We show that $\mathbf{z} := \text{sign}(a) \mathcal{F}_\Omega[\mathbf{w}_0^\top \gamma(\cdot)]_+ / \eta(\mathbf{w}_0)$ yields a valid dual certificate $\phi = \mathcal{L}_\Omega \mathbf{z}$ for the measure $\mu = a \delta_{\mathbf{w}_0}$.

First, observe that for all $\mathbf{w} \in \mathcal{U}_\eta$ we have

$$\phi(\mathbf{w}) = \text{sign}(a) \eta(\mathbf{w}_0)^{-1} \langle \mathcal{F}_\Omega[\mathbf{w}^\top \gamma(\cdot)]_+, \mathcal{F}_\Omega[\mathbf{w}_0^\top \gamma(\cdot)]_+ \rangle$$

Plugging in $\mathbf{w} = \mathbf{w}_0$, we see that

$$\phi(\mathbf{w}_0) = \text{sign}(a) \eta(\mathbf{w}_0)^{-1} \|\mathcal{F}_\Omega[\mathbf{w}_0^\top \gamma(\cdot)]_+\|_2 = \text{sign}(a) \eta(\mathbf{w}_0).$$

Also, by the Cauchy-Schwartz inequality, we have

$$|\phi(\mathbf{w})| \leq \eta(\mathbf{w}_0)^{-1} \|\mathcal{F}_\Omega[\mathbf{w}^\top \gamma(\cdot)]_+\|_2 \|\mathcal{F}_\Omega[\mathbf{w}_0^\top \gamma(\cdot)]_+\|_2 = \eta(\mathbf{w})$$

for all $\mathbf{w} \in \mathcal{U}_\eta$, with strict inequality when $\mathcal{F}_\Omega[\mathbf{w}^\top \gamma(\cdot)]_+$ is not co-linear with $\mathcal{F}_\Omega[\mathbf{w}_0^\top \gamma(\cdot)]_+$. Therefore, it suffices to show that when $\mathbf{w} \neq \mathbf{w}_0$ these vectors of Fourier coefficients cannot be co-linear.

Towards this end, suppose $\mathcal{F}_\Omega[\mathbf{w}^\top \gamma(\cdot)]_+ = c \mathcal{F}_\Omega[\mathbf{w}_0^\top \gamma(\cdot)]_+$ for some $c \in \mathbb{R}$. First, note that $\mathcal{F}\{[\mathbf{w}^\top \gamma(\cdot)]_+\}[\mathbf{0}] = \int_{[0,1]^d} [\mathbf{w}^\top \gamma(\cdot)]_+ dx > 0$ for all $\mathbf{w} \in \mathcal{U}_\eta$, since otherwise this would imply $[\mathbf{w}^\top \gamma(\cdot)]_+$ is identically zero. Therefore, $c = \mathcal{F}\{[\mathbf{w}^\top \gamma(\cdot)]_+\}[\mathbf{0}] / \mathcal{F}\{[\mathbf{w}_0^\top \gamma(\cdot)]_+\}[\mathbf{0}] \geq 0$. By linearity of \mathcal{F}_Ω and positive 1-homogeneity of the ReLU activation, we have $\mathcal{F}_\Omega[\mathbf{w}^\top \gamma(\cdot)]_+ = \mathcal{F}_\Omega[c \mathbf{w}_0^\top \gamma(\cdot)]_+$. However, by injectivity of the map $\mathbf{w} \mapsto \mathcal{F}_\Omega[\mathbf{w}^\top \gamma(\cdot)]_+$ as established in Lemma 5, we see this implies $\mathbf{w} = c \mathbf{w}_0$, and since we assume $\eta(\mathbf{w}) = \eta(\mathbf{w}_0) = 1$, by positive 1-homogeneity of η this can be the case if and only if $c = 1$, and so $\mathbf{w} = \mathbf{w}_0$. Therefore, if $\mathbf{w} \in \mathcal{U}_\eta$ is such that $\mathbf{w} \neq \mathbf{w}_0$ then $\mathcal{F}_\Omega[\mathbf{w}^\top \gamma(\cdot)]_+$ is not co-linear with $\mathcal{F}_\Omega[\mathbf{w}_0^\top \gamma(\cdot)]_+$, and so $|\phi(\mathbf{w})| < 1$. Therefore, we have shown ρ is a dual certificate for the measure $\mu = a[\mathbf{w}_0]_+$, and so by Lemma 4, it is the unique minimizer of (13), and hence f is the unique function space minimizer of (3). \square